Available online at www.sciencedirect.com

ScienceDirect

Acta Materialia 80 (2014) 56–66

Acta MATERIALIA

www.elsevier.com/locate/actamat

A critical assessment of the "stable indenter velocity" method for obtaining the creep stress exponent from indentation data

J. Dean [a,b], J. Campbell [a], G. Aldrich-Smith [c], T.W. Clyne [a,*]

[a] Department of Materials Science and Metallurgy, University of Cambridge, 27 Charles Babbage Road, Cambridge CB3 0FS, UK
[b] Double Precision Consultancy, Salisbury House, Station Road, Cambridge CB1 2LA, UK
[c] AWE, Aldermaston, Reading, UK

Received 7 May 2014; received in revised form 23 July 2014; accepted 24 July 2014
Available online 24 August 2014

Abstract

A technique for evaluating the (steady-state) creep stress exponent (n) from indentation data has come into common use over recent years. It involves monitoring the indenter displacement history under constant load and assuming that, once its velocity has stabilized, the system is in a quasi-steady state, with Stage II creep dominating the behaviour. The stress field under the indenter, and the way in which the creep strain field is changing there, are then represented by "equivalent stress" and "equivalent strain rate" values. These are manipulated in a similar manner to that conventionally employed with (uniaxial) creep test data, allowing the stress exponent, n, to be obtained as the gradient of a plot of the logarithm of the equivalent strain rate against the logarithm of the equivalent stress. The procedure is therefore a very simple one, often carried out over relatively short timescales (of the order of 1 h or less). However, concerns have been expressed about its reliability, regarding the neglect of primary creep (after a very short initial transient) and about the validity of representing the stress and strain rate via these "equivalent" values. In this paper, comprehensive experimental data (both from a conventional, uniaxial loading set-up and from instrumented indentation over a range of conditions) are presented for two materials, focusing entirely on ambient temperature testing. This is supplemented by predictions from numerical (finite element method) modelling. It is shown that the methodology is fundamentally flawed, commonly giving unreliable (and often very high) values for n. The reasons for this are outlined in some detail. An attempt is made to identify measures that might improve the reliability of the procedure, although it is concluded that there is no simple analysis of this type that can be recommended.

Keywords: Nanoindentation; Finite element analysis; Creep

1. Introduction

While the Young's modulus can readily be measured via instrumented indentation, obtaining plasticity parameters from indentation data is slightly more complex. Nevertheless, the yield stress and the initial work-hardening rate of a material can be inferred from indentation load–displacement relationships, using inverse, iterative finite element methods [1–10]. A considerably greater challenge is presented when attempting to obtain creep characteristics from indentation tests, partly because the number of parameters involved is greater – particularly if it is accepted that primary creep is likely to affect the observed behaviour. Furthermore, it is evident that the experimental data must encompass the time dependence of the behaviour. Nevertheless, the main issues involved have been addressed [11–15] and appropriate inverse, finite element method (FEM)-based methodologies have been proposed [16], although they are not simple to implement.

In parallel with these developments, there is a widely practised methodology for derivation of the stress

* Corresponding author.
E-mail address: twc10@cam.ac.uk (T.W. Clyne).

http://dx.doi.org/10.1016/j.actamat.2014.07.054
1359-6454/

exponent for (secondary) creep (n) from instrumented indentation data. These experiments are commonly carried out over relatively short timescales and the analysis is very straightforward. It involves identifying "equivalent" values for the stress and strain rate, and also assuming that Stage II creep is rapidly established throughout the parts of the sample affecting the indenter response. However, there are serious concerns about the validity of these assumptions and about the reliability of the values obtained. Certainly there have been experimental studies [11,15,17,18] that have revealed major discrepancies between values of n obtained using this approach and via conventional creep testing, although there have also been instances where some agreement has been claimed [19–26]. Some workers [27–30] have obtained plausible results from indentation creep experiments, but only by using system-specific "conversion factors" to relate indentation-derived values of n to those obtained from conventional creep tests.

A common concern during creep testing is that the specimen microstructure (grain structure, dislocation density, precipitate dispersion etc.), which can significantly affect creep behaviour, may evolve in some way during the period of the test, possibly as a consequence of high plastic strains in the immediate vicinity of the indenter. If this were a potential explanation for discrepancies between indentation-derived and conventionally obtained creep parameters, then it might be expected that they would not arise with (metallic) glass samples (in which no microstructural evolution is expected to occur, assuming that there is no crystallization). However, experiments on Fe-based glasses [31] gave large discrepancies in the value of n, interpreted in terms of shear transformation zones. Tests on amorphous selenium [32], on the other hand, led to good agreement in some instances, although not in others.

In general, the picture is very confused and it is clear that this situation needs to be resolved, so that the reliability and limitations of the methodology become widely acknowledged. In the present paper, the procedure concerned is examined in some detail, both experimentally and theoretically, and conclusions are reached.

2. Background

2.1. Conventional creep testing

Secondary ("Stage II" or "steady state") creep is commonly found to become established after a certain time, with an approximately constant strain rate that often conforms to an equation of the form

$$\dot{\varepsilon}_{\text{creep}} = C\sigma^n \exp\left(\frac{-Q}{RT}\right) \tag{1}$$

where C is a constant, σ is the (uniaxial) stress, n is the stress exponent, T is the absolute temperature and Q is an activation energy. The stress is normally uniform throughout the (gauge length of the) sample and most tests are carried out with its value maintained constant. The stress exponent, n, can be obtained from a plot of $\ln\dot{\varepsilon}$ against $\ln\sigma$. The value of Q can be found from a plot of $\ln\dot{\varepsilon}$ against $1/T$. Eq. (1) is essentially an empirical relationship, although it is sometimes possible to rationalize the observed values of n and Q in terms of some model for the rate-determining process taking place within the microstructure of the material.

2.2. Indentation creep testing

In contrast to conventional testing, indentation creates stress and strain fields that vary with position and time. Furthermore, indentation tests are commonly conducted over relatively short periods – often measured in minutes – whereas conventional tests usually run for many hours (or weeks). A commonly employed procedure for obtaining a value of n is based on the following equation:

$$\frac{1}{h}\frac{\mathrm{d}h}{\mathrm{d}t} = C\left(\frac{P}{A_{\text{p}}(h)}\right)^n \exp\left(\frac{-Q}{RT}\right) \tag{2}$$

where h is the indentation depth, $(\mathrm{d}h/\mathrm{d}t)$ is the velocity of the indenter (during a "creep dwell" period), P is the indenter load (held constant during the "creep dwell" period) and $A_{\text{p}}(h)$ is the projected contact area between indenter and specimen (as a function of h). Comparing this equation with Eq. (1), it can be seen that the following assumptions are incorporated into the approach:

(1) At any time, the stress field beneath the indenter can be represented by a single "equivalent" value (given by the load over the current projected contact area).
(2) At any time, the changing strain field beneath the indenter can be represented by a single "indentation" creep strain rate (given by the current indenter velocity over the current depth).
(3) Once the indenter velocity has become (approximately) constant, "Stage II" creep is fully established throughout all the parts of the sample affecting the indenter penetration (and primary creep can be ignored).

3. Experimental procedures

3.1. Materials

Two materials were employed. The first was an oxygen-free, high conductivity copper, received in extruded rod form (12 mm diameter). Specimens for metallographic investigation were cut from the rod using electric discharge machining (EDM), mechanically polished and etched with dilute ferric chloride. The microstructure can be seen in Fig. 1a. The copper has a relatively fine grain size, with an average grain diameter of ~15–20 μm.

The second material studied was pure tin (99.99+%). Tin shot was melted in an alumina crucible and cast into a cylindrical mould (5.8 mm diameter) submerged in liquid

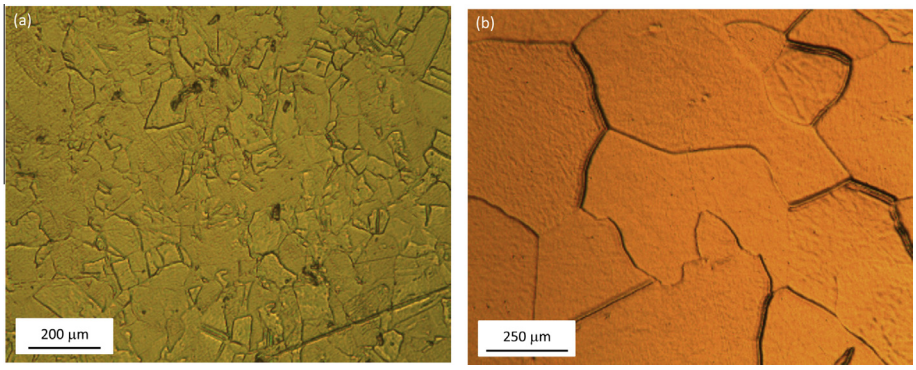

Fig. 1. Optical micrographs showing the grain structures of (a) oxygen-free, high conductivity copper and (b) cast tin.

nitrogen. Specimens for metallographic examination were cut from cast rods, using a diamond-tipped circular saw. The tin microstructure (unetched) is shown in Fig. 1b. It can be seen that the grain structure is coarse, with typical grain diameters in the 300-400 μm range.

3.2. Compression testing

All tests were conducted at room temperature (~20 °C), corresponding to homologous temperatures of 0.22 and 0.58, respectively, for the Cu and Sn. These two materials are thus expected to encompass a wide range of creep rates (depending on the applied stress level). Yielding characteristics (yield stress and work-hardening rate) of the Cu were measured in compression, using a 100 kN servo-hydraulic machine. The Cu cylinders were compressed between flat platens of silicon carbide, lubricated to minimize barrelling. Displacements were measured using a linear variable displacement transducer, with a precision of ~±2 μm. Loading was along the extrusion axis. The tin was similarly tested (loaded along the axis of the cylindrical casting), using a 2.5 kN, screw-driven machine. Displacements were measured using a scanning laser extensometer with a resolution of ~±1 μm.

3.3. Conventional (uniaxial) creep testing

Cylindrical Cu specimens (4 mm height, 3 mm diameter) were CNC-machined from extruded rod and tested in compression under constant stress (applied via dead weights). Tests were conducted with three different stress levels (222, 259 and 297 MPa). This range covers values close to (but not exceeding) the yield stress of the Cu, in recognition of the fact that, during indentation, the deviatoric (von Mises) stress beneath the indenter is likely to be close to uniaxial yield stress. Displacements were measured using a scanning laser extensometer with a resolution of ~±3 μm. Cylindrical Sn specimens (6 mm height, 5.8 mm diameter) were cut from cast rods using a diamond-tipped, circular saw. Creep tests were conducted in compression, in a similar manner to that of the Cu samples, with stress levels of 6.96, 7.08, 8.05 and 8.86 MPa (also covering values close to, but not exceeding, the yield stress). It is recognized that these two sets of tests did not allow the value of n to be established with high precision. However, the use of a wider range of stress levels might have risked encompassing more than a single regime of creep mechanism. Moreover, as will shortly become clear, it was not necessary for present purposes to obtain a highly accurate value for n.

3.4. Indentation creep testing

It is recognized [10] that reproducibility and capture of the macroscopic mechanical characteristics are improved by ensuring that the indent size is appreciably larger than the grain size. Three scales of indentation have been employed in the current work: nanoindentation, microindentation and macroindentation. The type of test employed was determined primarily by this requirement to interrogate a representative volume (containing multiple grains). The effects of tip shape, tip size, applied load, loading rate and creep dwell time on indentation-derived values of n are all of interest and these parameters were systematically varied during the experiments. Test matrices for the Cu and the Sn are presented in Tables 1 and 2.

The tests were all carried out with the indenter moving in the axial direction of the (cylindrical) sample. This was the extrusion direction for the copper rod and the casting axis for the tin samples. These tests were therefore conducted along the same direction as the corresponding compression tests. The samples were mechanically polished down to 1 μm diamond level before testing. Indents were distributed randomly around the section. It was confirmed in trials that the location of the indent had no apparent effect on the outcome (although there was noticeable scatter if the indent did not straddle at least several grains).

Drift rates were monitored during hold periods of duration equal to those of the creep tests. Measured drift rates were small and linear in all instances (<0.02 nm s^{-1}), which is unsurprising for tests carried out at ambient temperature. These rates were of no consequence for the microindentation and macroindentation experiments, but nanoindentation data are presented after these (small) drift corrections.

Table 1
Test conditions for indentation of copper samples.

Test number	Machine	Indenter shape	Indenter radius (μm)	Loading rate (mN s^{-1})	Maximum applied load (mN)	Creep dwell period (s)	Derived value of n
1	Nanoindenter	Sphere	25	100	500	60	33
2	Nanoindenter	Sphere	25	100	500	600	29
3	Nanoindenter	Sphere	25	100	500	3600	21
4	Nanoindenter	Sphere	50	100	500	60	33
5	Nanoindenter	Sphere	50	100	500	600	23
6	Nanoindenter	Sphere	50	100	500	3600	18
7	Nanoindenter	Berkovich	N/A	100	500	60	80
8	Nanoindenter	Berkovich	N/A	100	500	600	56
9	Nanoindenter	Berkovich	N/A	100	500	3600	15
10	Microindenter	Sphere	796	20	5000	600	15
11	Microindenter	Sphere	796	20	5000	1800	8
12	Microindenter	Sphere	796	20	5000	3600	6
13	Microindenter	Sphere	796	50	5000	600	16
14	Microindenter	Sphere	796	50	5000	1800	9
15	Microindenter	Sphere	796	50	5000	3600	7
16	Microindenter	Sphere	796	100	5000	600	18
17	Microindenter	Sphere	796	100	5000	1800	11
18	Microindenter	Sphere	796	100	5000	3600	9
19	Microindenter	Sphere	796	20	10,000	600	46
20	Microindenter	Sphere	796	20	10,000	1800	24
21	Microindenter	Sphere	796	20	10,000	3600	16
22	Microindenter	Sphere	796	50	10,000	600	16
23	Microindenter	Sphere	796	50	10,000	1800	9
24	Microindenter	Sphere	796	50	10,000	3600	7
25	Microindenter	Sphere	796	100	10,000	600	15
26	Microindenter	Sphere	796	100	10,000	1800	9
27	Microindenter	Sphere	796	100	10,000	3600	7
28	Microindenter	Sphere	796	20	20,000	600	23
29	Microindenter	Sphere	796	20	20,000	1800	11
30	Microindenter	Sphere	796	20	20,000	3600	4
31	Microindenter	Sphere	796	50	20,000	600	14
32	Microindenter	Sphere	796	50	20,000	1800	7
33	Microindenter	Sphere	796	50	20,000	3600	5
34	Microindenter	Sphere	796	100	20,000	600	16
35	Microindenter	Sphere	796	100	20,000	1800	10
36	Microindenter	Sphere	796	100	20,000	3600	8

4. Finite element modelling

4.1. Meshing and mechanical boundary conditions

Axisymmetric finite element models were built in ABAQUS/CAE, based on radial symmetry. The Berkovich tip was modelled as a cone with an apex semi-angle of 70.3°, which gives the same projected contact area for a given depth as the true Berkovich. All of the indenters were modelled as analytical rigid bodies. Specimens were modelled as deformable bodies and meshed with linear (type CAX3) triangular elements. The meshes were refined in regions directly beneath the indenter, in order to handle the high gradients of stress, strain and strain rate. Sensitivity analyses confirmed that the meshes were sufficiently fine to achieve convergence, numerical stability and mesh-independent results. Contact between the indenters and the specimens was taken as frictionless. Experimentally measured loading histories were specified as boundary conditions at the indenter. Resultant indenter displacement histories were recorded as an outcome (solution) of the modelling.

4.2. Constitutive representation of material behaviour

Young's moduli of 122 and 42 GPa, respectively, were specified for the Cu and Sn. (These values are taken from the literature, but they are very close to those obtained from the initial parts of unloading curves during indentation.) The yield stress and work-hardening characteristics were obtained experimentally and plots of stress against plastic strain are shown in Fig. 2. The Cu yields at ~327 MPa. Beyond a strain of 10%, the Cu was assumed to harden linearly, with a work-hardening rate of 437 MPa. The tin has a yield stress of 12 MPa and a (linear) work-hardening rate of 84 MPa.

Measured plots of creep strain against time are shown in Fig. 3a for the Cu. The curves exhibit the characteristic traits of both primary (Stage I) and steady state (Stage II) creep, i.e. the creep strain rates are initially high, falling with time until a steady state (minimum) creep strain rate is reached. It is clear that, in all instances, the primary creep regimes extend over significant periods of time – typically several hours – before a steady-state is established.

Table 2
Test conditions for indentation of tin samples.

Test number	Machine	Indenter shape	Indenter radius (mm)	Loading rate (mN s^{-1})	Maximum applied load (N)	Creep dwell period (s)	Derived value of n
37	ESH 5 kN Hounsfield	Sphere	1.58	0.3	150	60	29
38	ESH 5 kN Hounsfield	Sphere	1.58	0.3	150	600	19
39	ESH 5 kN Hounsfield	Sphere	1.58	0.3	150	1800	17
40	ESH 5 kN Hounsfield	Sphere	1.58	0.3	150	3600	16
41	ESH 5 kN Hounsfield	Sphere	1.58	3.0	150	60	14
42	ESH 5 kN Hounsfield	Sphere	1.58	3.0	150	600	13
43	ESH 5 kN Hounsfield	Sphere	1.58	3.0	150	1800	13
44	ESH 5 kN Hounsfield	Sphere	1.58	3.0	150	3600	14
45	ESH 5 kN Hounsfield	Sphere	1.58	30	150	60	13
46	ESH 5 kN Hounsfield	Sphere	1.58	30	150	600	15
47	ESH 5 kN Hounsfield	Sphere	1.58	30	150	1800	16
48	ESH 5 kN Hounsfield	Sphere	1.58	30	150	3600	18

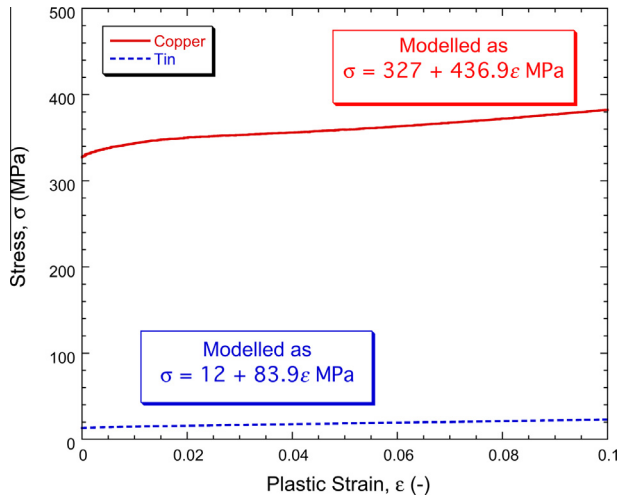

Fig. 2. Experimental stress–strain plots for uniaxial compression testing of Cu and Sn samples, plus the expressions used to represent this behaviour in the FEM model.

The complete creep strain histories in Fig. 3a were modelled using the Miller–Norton creep equation:

$$\varepsilon_{\text{creep}} = \frac{C\sigma^n t^{m+1}}{m+1} \tag{3}$$

The stress exponent, n, was obtained by plotting the natural logarithm of the steady-state creep strain rate against the natural logarithm of the applied stress, as in Fig. 3b. The parameters C and m are material constants, with best fit values of 3.22×10^{-12} $\text{MPa}^{-n}\,\text{s}^{-(m+1)}$ and -0.81, respectively. It can be seen that the modelled curves are a good representation of the experimental data. A form of the Miller–Norton creep equation was implemented in ABAQUS, in which the cumulative creep strain (and not the time) was used to define the current "state" of the material:

$$\dot{\varepsilon}_{\text{creep}} = \left\{C\sigma^n[(m+1)\varepsilon_{\text{creep}}]^m\right\}^{\left(\frac{1}{m+1}\right)} \tag{4}$$

Included in Fig. 3a are a further set of modelled curves obtained using the steady-state creep equation

$$\dot{\varepsilon}_{\text{creep}} = B\sigma^n. \tag{5}$$

In this equation, the creep strain rate is constant (independent of time and strain), depending only on the values of B and n. This is a more suitable representation of the steady-state creep strain rate than Eq. (1), since the activation energy is unknown and only a single test temperature has been used. The best-fit value of B is 2.24×10^{-16} $\text{MPa}^{-n}\,\text{s}^{-1}$, for n fixed at its measured value of 3.5; see Fig. 3b.

The corresponding plots to those of Fig. 3 for the Sn case are shown in Fig. 4. It can be seen in Fig. 4b that the deduced value of n is 4.3. The best fit values of C, B and m are respectively 1.1×10^{-7} $\text{MPa}^{-n}\,\text{s}^{-(m+1)}$, 3.2×10^{-10} $\text{MPa}^{-n}\,\text{s}^{-1}$ and -0.665. Again, the Miller–Norton expression (Eq. (3)) provides a good approximation of the experimental behaviour.

In general, it may be concluded that, for both the copper and the tin samples, the creep characteristics (in what might be described as the "high stress" domain) have been reliably captured, with primary creep dominating for the

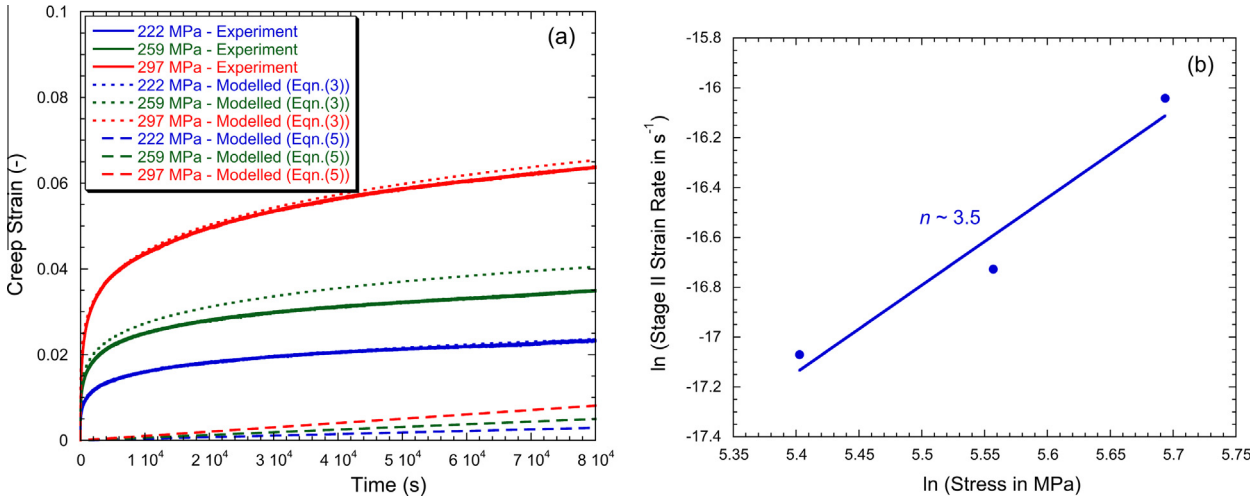

Fig. 3. (a) Measured and modelled creep strain histories for Cu, with three different stress levels, and (b) plot of the logarithm of (steady state) strain rate against the logarithm of stress, showing the derived value of the stress exponent.

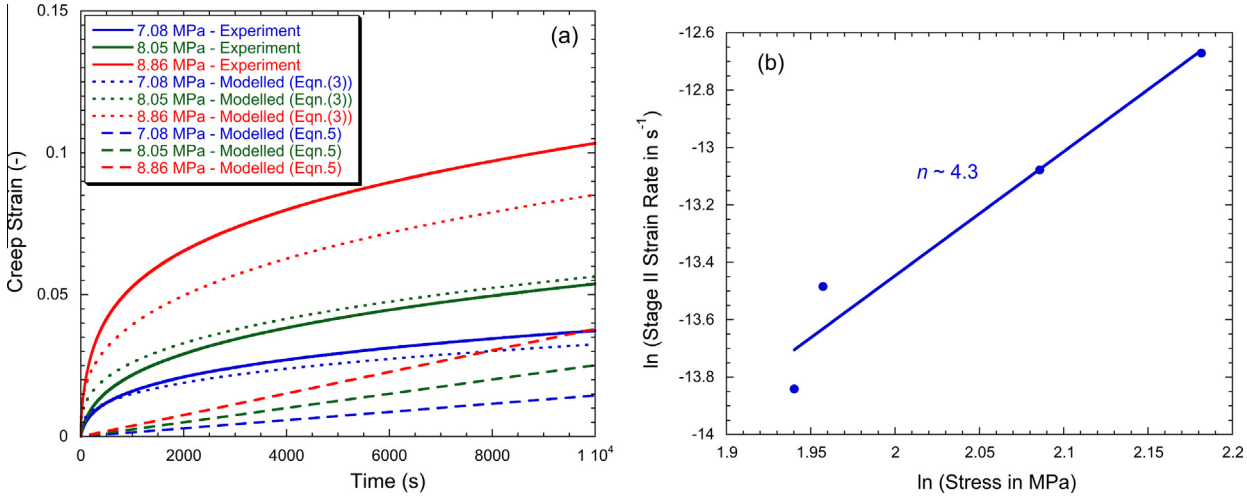

Fig. 4. (a) Measured and modelled creep strain histories for Sn, with three different stress levels, and (b) plot of the logarithm of (steady state) strain rate against the logarithm of stress, showing the derived value of the stress exponent.

first few hours, after which a steady state is established, in which the stress exponent, n, has a value of the order of 4.

5. Evaluation of n from indentation creep dwell curves

5.1. Creep dwell curves for copper

A selection of representative creep dwell curves for testing of Cu is presented in Fig. 5a. (The details of each case are provided in Table 1.) These plots have been chosen to cover a range of indenter shape, size and indentation loading rate. The curves for tests 9, 30 and 33 appear to enter a "steady-state" (approximately constant indenter velocity) after ~10 min. This is an important observation, since the analysis of Section 2.2 is predicated on the assumption that a constant indenter velocity has been attained and that this is indicative of steady-state creep occurring throughout the deforming volume. In contrast, the velocity for test 6 continues to fall throughout the creep dwell period and a "steady state" is not established. Nevertheless, in Fig. 5b, the methodology of Section 2.2 has been applied to the creep dwell curves of Fig. 5a. Linear curves have been fitted to the last 360 s of data (last 10%) – i.e. the lower parts each data set, in order to generate values for n. This process was repeated for each of the tests listed in Table 1.

There are several noteworthy features, the most obvious being the poor level of agreement in almost all instances between the indentation-derived and the macroscopically measured value of n (~3.5). Many of the values (those of tests 1–10, 13, 16, 19–22, 25 and 28) are very large (>~15). To put such values into some kind of context, a stress exponent value of 18 (test 16) implies that a 20% increase in the stress level would raise the (steady state) creep strain rate by a factor of ~30, while a value of 25

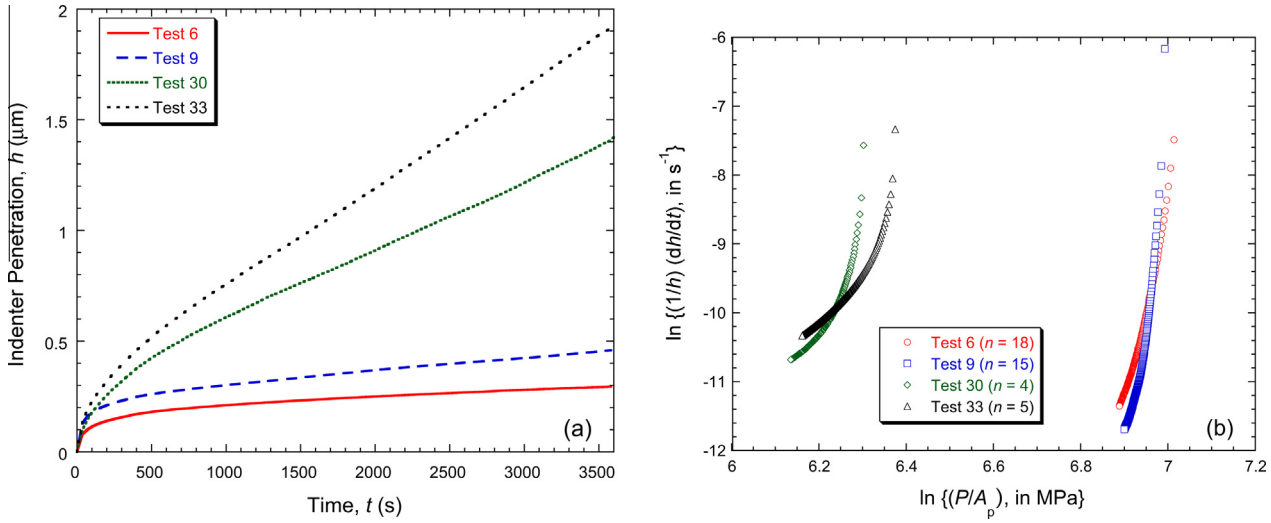

Fig. 5. Data from four constant load indentation creep tests on Cu: (a) experimental displacement–time plots and (b) corresponding plots of the logarithm of the "effective" (steady state) strain rate against the logarithm of the "effective" stress, showing the derived values of the stress exponent.

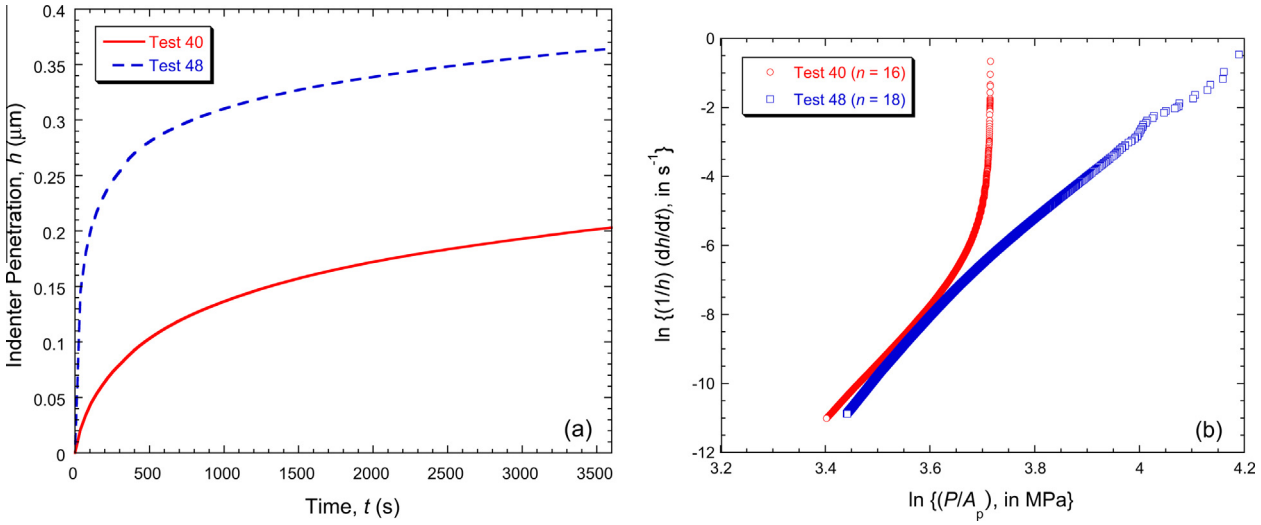

Fig. 6. Data from two constant load indentation creep tests on Sn: (a) experimental displacement–time plots and (b) corresponding plots of the logarithm of the "effective" (steady state) strain rate against the logarithm of the "effective" stress, showing the derived values of the stress exponent.

would imply an increase by a factor of almost 100. It is difficult to imagine how such extreme sensitivity to stress could possibly arise and very doubtful if such sensitivities have ever been recorded in conventional creep testing. These physically implausible values of n are at least partly due to high indenter velocities arising during the creep dwell period as a consequence of it being largely dominated by primary creep and not, therefore, amenable to a "steady-state" type analysis.

It is also worth noting that, at least for the data from tests 30 and 33 in Fig. 5b, the value of n that would be obtained falls throughout the test. Furthermore, towards the end of the test, the value is starting to approach its "correct" value (of 3.5), which at least appears to offer some encouragement that the procedure can under some circumstances lead to reliable results. In fact, it can be seen from Table 1 (and Table 2, for the Sn data), that these are the only tests for which the value of n is in the correct range. These two tests employed a large diameter (~1.6 mm) spherical indenter, a slow initial loading rate, a large creep load and a relatively long creep period. There are reasons for expecting all of these factors to move the measurements in the right direction. However, it can also be seen in Table 1 that there is a large scatter in the obtained values of n, even when some or all of those steps are taken.

Furthermore, the derived values of n appear to be sensitive to tip shape. This should not be the case, provided the stress states are not so dissimilar that alternative mechanisms of creep could be stimulated. This seems unlikely, since the stress state during indentation (for all tip shapes) tends to involve high deviatoric stresses, such that the mechanism of creep is likely to be dislocation-affected for all indenter shapes. Indeed, it may well be the case that

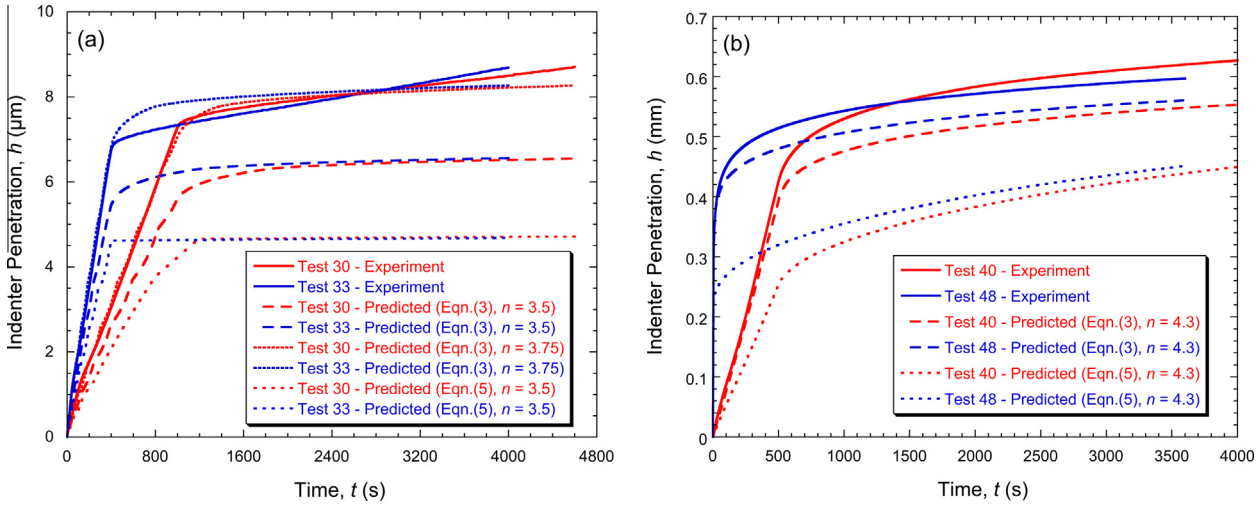

Fig. 7. Comparisons between experimental and predicted indenter penetration histories for a pair of tests carried out on (a) Cu and (b) Sn samples.

indentation is inherently unsuited to obtaining creep data in what might be described as the "low stress, long time-scale" regime.

5.2. Creep dwell curves for tin

Creep dwell curves for tin, from tests 40 and 48, are shown in Fig. 6. The differences between these two are due to the difference in the loading ramp rate prior to the creep dwell period, which was 0.3 N s^{-1} in test 40 and 30 N s^{-1} in test 48. A low rate leads to some creep occurring during the load ramping phase, allowing stress relaxation during this period and reducing the rate of creep during the initial part of the creep dwell period. It can be seen, however, that the creep rates become similar after a while and similar values are obtained for n, although these values are again very high (and much greater than the "correct" value for the Sn, which is ~4.3). Further derived values of n are shown in Table 2, where it can be seen that all of these cases gave very high n values. It can be seen in Fig. 4 that the "Stage I (primary creep) period" is around 1 or 2 h for the Sn, whereas it is several hours for the Cu (Fig. 3). This might be consistent with the fact that the Sn tests listed in Table 2 all tend to converge to a similar value of n after relatively short periods (corresponding to Stage II creep becoming predominant), although this value (~15-20 in most cases) is well above the "correct" value. It may also be noted that, as penetration proceeds and the (creep) strain field expands, there will always be regions experiencing primary creep (although the influence that they have on the indenter velocity is indeterminate without further information).

6. Critical appraisal of the methodology

6.1. Primary creep

The analysis of Section 2.2 (Eq. (2)) is based on the assumption that, at any time, the "equivalent creep strain rate" in any deforming volume element is the minimum (steady state) value for its current "equivalent stress". It is thus assumed that primary creep can be neglected, and that a true steady state (in terms of creep deformation) is instantly attained.

The validity of this assumption is examined in Fig. 7a, in which experimental data from tests 30 and 33 are compared to FEM predictions. Three predicted curves are shown in each case. The first pair of predictions was obtained using the Miller–Norton creep equation (Eqs. (3) and (4)) and the best fit parameters of Fig. 3a. The second pair of predictions was obtained using the same equation, but employing a value of 3.75 for n (representing a 7% increase on 3.5). The level of agreement between the measured and predicted curves improves substantially when this change is made, highlighting the sensitivity of the predictions to the stress exponent, n. In fact, the sensitivity of the creep strain rate to small changes in C, n and m is such that quite small deviations between their real and approximated values may generate predictions that are markedly different. Recognizing this, the level of agreement between experimental data and model predictions in Fig. 7a is encouraging.

The third pair of predicted curves in Fig. 7a was obtained using the steady-state creep equation (Eq. (5)) and the best fit value of B from Fig. 3a. These predictions were obtained by assuming that, in all volume elements, the steady-state creep strain rate is instantaneously adopted, corresponding to the instantaneous local stress, and is maintained for the duration of each time increment. This procedure therefore takes account of the changing stress field within the specimen, making it more rigorous than the analysis of Section 2.2, but takes no account of primary creep. It can be seen that the predicted amount of creep is well below that observed experimentally and it is clear that neglect of primary creep introduces a very large error.

In Fig. 7b, corresponding information is presented for a pair of tests carried out on Sn samples, with only the "correct" value of n being employed. In this case the creep rates are appreciably higher than for the Cu samples, but similar conclusions can be drawn.

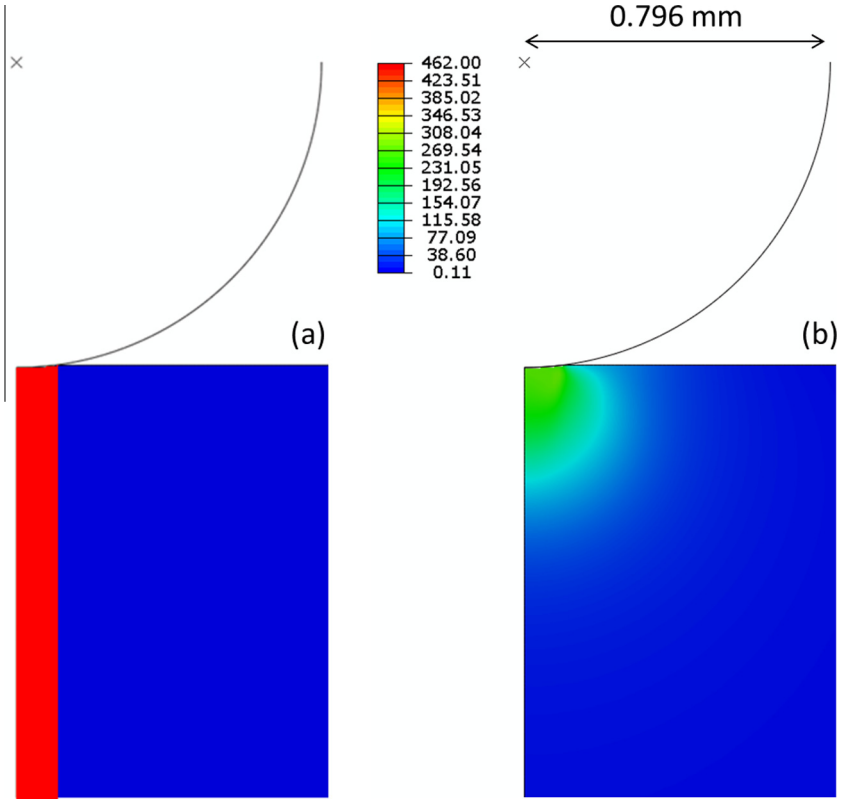

Fig. 8. Predicted (von Mises) stress fields under an indenter. The case treated is that of test 30, after a 1 h creep period. The fields shown are those obtained (a) using the "equivalent stress" assumption and (b) from the FEM model. The stress levels in the legend are in MPa.

6.2. Equivalent stress

The assumption that the stress field underneath an indenter can be treated as if it were uniform in a column with the projected area of contact as its section, with a value equal to the load divided by this sectional area, is clearly a rather crude one. In fact, it will in general be some considerable way from reality, irrespective of whether the stress field is elastic, elasto-plastic or creep-affected. The distortion represented by the assumption is illustrated by Fig. 8, in which a comparison is presented (for one of the test cases studied here) between the assumed field (Fig. 8a) and the actual (FEM predicted) one (Fig. 8b). The calculated value for the equivalent stress in this case is 462 MPa. The FEM prediction indicates that the actual (von Mises) stress levels are much lower, and of course they are distributed over a wider area under the indenter. It is evident that use of the equivalent stress in any analytical framework is likely to cause large errors to arise.

6.3. Equivalent strain rate

The other main assumption made in the method concerning the stress and strain field involves representing the creep response of the material by an "effective" creep strain rate (of $(1/h)(\mathrm{d}h/\mathrm{d}t)$). Comparisons are shown in Fig. 9 between the value of this expression, for a particular test after two different times, and the strain rate (rate of change of the equivalent, or von Mises, strain) field predicted using the FEM model. It can be seen that the "effective" value is in both cases about an order of magnitude greater than the peak value predicted by the model. Moreover, that peak value is generated only in a very small fraction of the region under the indenter, most of which is experiencing considerably smaller strain rates. These observations are broadly representative of the situations created over a wide range of test conditions.

6.4. Combined effects

It can thus be seen that, for both of the "equivalent" parameters employed in the method, the values being employed are much larger than the peak values created in reality. Furthermore, the difference is substantially greater if the comparison is with some sort of average value over the region influencing the indenter response. It is possible that, at least in some cases, the fact that both of these parameters are being grossly overestimated could have a compensatory effect, since they appear on opposite sides of the equation concerned. However, in view of the sensitivity of the creep behaviour to n, it is very unlikely that this would lead to any kind of reliable measurement of its value – which is, of course, consistent with the huge scatter in the values obtained experimentally in the present work. The other prominent feature of the experimental outcomes is that there is a strong tendency for the value

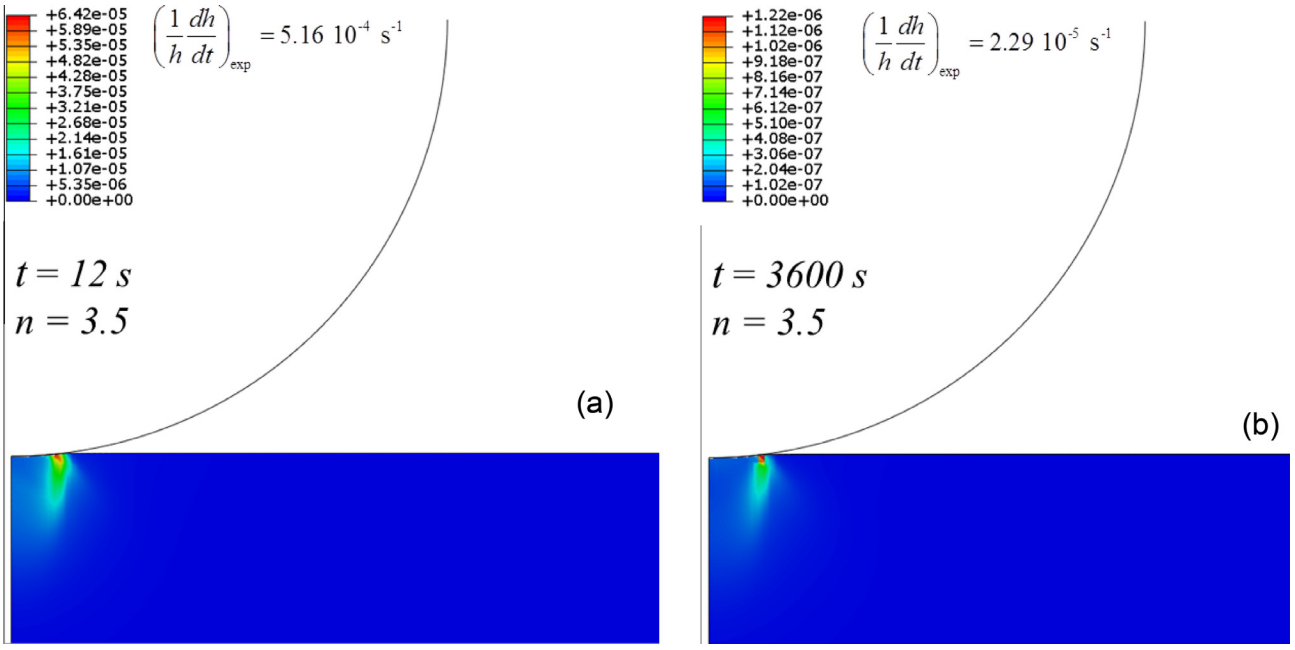

Fig. 9. Predicted (creep) strain rate fields under an indenter. The case treated is that of test 30. The fields shown are those after creep dwell times of (a) 12 s and (b) 3600 s. The strain rate levels in the legend are in s^{-1}. The corresponding value of the expression for the "equivalent strain rate", obtained using experimental data, is also shown in each case.

of n to be overestimated (rather than underestimated). It seems likely that this trend is at least largely due to the neglect of primary creep, which accelerates the creep rates (and thus (dh/dt)), raising the value of the gradient of the plot of $\ln[(1/h)(dh/dt)]$ against $\ln[P/(A_p(h))]$ and hence giving an enhanced value of n.

7. Conclusions

The following conclusions can be drawn from this work, which is focused on a commonly used methodology for obtaining creep stress exponent (n) values from indentation data – using experimental measurements of the indenter velocity, which often exhibits a tendency to stabilize quite quickly.

(a) It has been shown, by applying the methodology to creep indentation tests carried out with almost 50 different sets of conditions (on two different materials), that the derived values of n exhibit a huge degree of scatter (from ~4 to ~50). The "correct" values of n for the two materials (obtained via conventional creep testing) are ~3.5 and 4.5. In addition to the scatter, therefore, there is a strong tendency for the value of n to be overestimated. Such trends have been reported quite extensively in previous work.

(b) FEM modelling has been used to demonstrate that these effects, and the general unreliability of the methodology, are mainly caused by three (inaccurate) assumptions. The first of these is the neglect of primary creep. In practice, it is virtually impossible to eliminate the effect of primary creep during indentation testing, since, even if relatively long timescales are used in the tests, the volume of material undergoing creep is constantly expanding and hence some of it will always be creeping in the primary regime. In fact, it seems likely that, in many of the creep indentation experiments carried out hitherto, all of the creeping part of the sample has been in the primary regime throughout the test. Primary creep is in general expected to lead to an overestimate of the value of n if the methodology is used.

(c) The other two key assumptions, which probably also contribute to the observed scatter in the derived value of n, involve ascribing "equivalent" values to the magnitudes of the stress and of the creep strain rate in the indented region. It has been shown that both of these "equivalent" values are in all cases considerably larger than the peak magnitudes actually generated within the material and substantially greater than any kind of volume-averaged value.

(d) An attempt has been made to identify test regimes in which the errors are likely to be less significant. It is concluded that a large indenter, a high creep load, a slow ramping of the load up to the "creep dwell" level and a long test period may all help somewhat. However, it should be emphasized that there would appear to be no combination of conditions likely to yield acceptable results. A logical approach, if a fine scale test is required, would appear to be testing of micro-pillars, which is expected to lead to the "equivalent" values being closer to reality and the regime dominated by primary creep to be easier to identify. However, this introduces various other difficulties,

complications and errors. The best solution is almost certainly to employ a modelling procedure taking account of the actual stress and strain fields, and the contribution of primary creep, in which case the testing can be done on a fine scale, using a flat bulk specimen and within fairly short timescales. It is clear that this requires numerical modelling, which cannot be reduced to the use of analytical equations.

Acknowledgements

This work has been supported by EPSRC and also by AWE, as part of an ongoing collaboration aimed at the development of robust and user-friendly tools for the extraction of mechanical property characteristics from instrumented indentation data.

References

[1] Dao M, Chollacoop N, Van Vliet KJ, Venkatesh TA, Suresh S. Acta Mater 2001;49:3899–918.
[2] Bouzakis K, Michailidis N. Thin Solid Films 2004;469:227–32.
[3] Bouzakis K, Michailidis N. Mater Character 2006;56:147–57.
[4] Lee H, Lee J, Pharr G. J Mech Phys Sol 2005;53:2037–69.
[5] Pelletier H. Tribol Int 2006;39:593–606.
[6] Kim J, Lee K, Lee J. Surf Coat Technol 2006;201:4278–83.
[7] Guelorget B, Francois M, Liu C, Lu J. J Mater Res 2007;22:1512–9.
[8] Lee K, Kim K, Kim J, Kwon D. J Phys D Appl Phys 2008;41. p. Art. 74014.
[9] Heinrich C, Waas AM, Wineman AS. Int. J. Solids Struct 2009;46:364–76.
[10] Dean J, Wheeler JM, Clyne TW. Acta Mater 2010;58:3613–23.
[11] Goodall R, Clyne TW. Acta Mater 2006;54:5489–99.
[12] Stone D, Jakes J, Puthoff J, Elmustafa A. J Mater Res 2010;25:611–21.
[13] Galli M, Oyen M. Int J Mater Res 2009;100:954–9.
[14] Cao Y. Mech Time-Depend Mater 2007;11:159–72.
[15] Chen W, Cheng Y, Li M. Mater Sci Eng A 2010;527:5613–8.
[16] Dean J, Bradbury A, Aldrich-Smith G, Clyne T. Mech Mater 2013;65:124–34.
[17] Frost HJ, Ashby MF. Deformation mechanism maps – the plasticity and creep of metals and ceramics. Oxford: Pergamon Press; 1982.
[18] Shen L, Cheong WCD, Foo YL, Chen Z. Mater Sci Eng A 2012;532:505–10.
[19] Mayo MJ, Siegel RW, Narayansamy A, Nix WD. J Mater Res 1990;5:1073–81.
[20] Raman V, Berriche R. J Mater Res 1992;7:627–38.
[21] Fujiwara M, Otsuka M. Mater Sci Eng A 2001;A319–321:929–33.
[22] Liu H, Chen Y, Tang Y, Wei S, Nuiu G. Mater Sci Eng A 2007;464:124–8.
[23] Takagi H, Dao M, Fujiwara M. Acta Mech Solida Sin 2008;21:283–8.
[24] Mahmudi R, Geranmayeh AR, Khanbareh H, Jahangiri N. Mater Des 2009;30:574–80.
[25] Mahmudi R, Pourmajidian M, Geranmayeh AR, Gorgannejad S, Hashemizadeh S. Mater Sci Eng A 2013;565:236–42.
[26] Marques VMF, Wunderle B, Johnston C, Grant PS. Acta Mater 2013;61:2471–80.
[27] Dorner D, Roller K, Skrotzki B, Stockhert B, Eggeler G. Mater Sci Eng A 2003;357:346–54.
[28] Liu YJ, Zhao B, Xu BX, Yue ZF. Mater Sci Eng A 2007;456:103–8.
[29] Xu BX, Wang XM, Zhao B, Yue ZF. Mater Sci Eng A 2008;478:187–94.
[30] Takagi H, Fujiwara M. Mater Sci Eng A 2014;602:98–104.
[31] Huang YJ, Shen J, Chiu YL, Chen JJJ, Sun JF. Intermetallics 2009;17:190–4.
[32] Su C, Herbert EG, Sohn S, LaManna JA, Oliver WC, Pharr GM. J Mech Phys Solids 2013;61:517–36.